Design and construction of a micro-indenter for tribological investigations

Entwicklung und Anwendung eines Mikroindenters für tribologische Untersuchungen

K. S. Tan, A. W. Hassel*, M. Stratmann

Characterisation of erosion contact conditions remains a challenge due to the chaotic morphology of eroded surfaces. The present work presents details on the design and construction of a low load micro-indenter to investigate the initial stages of particle impact. Spherical ZrO_2 particles and angular SiC particles have been fitted onto stainless steel indenter tips to simulate contact between eroding particles on an aluminium surface. Contact loads between 50 and 1800 mN were utilised to elucidate the effects of load and indentation depth. Indented craters were subsequently imaged by the scanning electron microscope (SEM), revealing its particle dependent morphology. Crater area and depths from both types of particles were also quantified and subsequently correlated to the indentation load. It was demonstrated that contact pressure generated by angular particles are 1.5 times higher than those from spherical particles, resulting in greater plastic deformation and larger crater area at high loads. The work carried out during indentations were also calculated, it was shown that indentation experiments can be utilised for simulating dynamic erosion experiments under a large velocity range.

Keywords: tribocorrosion, indentation, erosion, particle angularity, kinetic energy.

Die vollständige Beschreibung von Materialien unter Erosionsbedingungen ist auf Grund der komplexen oder gar chaotischen Zustände ausgesprochen schwierig. In der hier vorgestellten Arbeit wird die Konstruktion und Anwendung eines empfindlichen Mikroindenters zur Untersuchung der Wirkung von Partikeleinschlägen vorgestellt. Dieser gestattet sowohl die Verwendung kugelförmiger ZrO_2 als auch scharfkantiger SiC Partikel. Diese werden zwecks Verwendung auf einer Stahlnadel montiert und zur Untersuchung von Aluminiumoberflächen eingesetzt. Der Zusammenhang zwischen Indenterkraft und Eindrucktiefe wurde für Kräfte zwischen 50 und 1800 mN untersucht. Eine genaue Untersuchung von Größe und Morphologie der Eindrücke erfolgte rasterelektronenmikroskopisch. Die quantitative Auswertung von Indentfläche und –tiefe erfolgte für beide Partikelarten als Funktion der Kraft. Es konnte gezeigt werden, daß der Kontaktdruck im Fall der kantigen Partikel etwa 1.5 mal so hoch wie der der sphärischen Partikel ist. Dies zeigt sich bei höheren Kräften deutlich an den höheren plastischen Verformungen und den größeren Kraterdurchmessern. Die am Material geleistete Arbeit wurde berechnet um zu zeigen, daß sich die hier beschriebenen statischen Indenterversuche in einem weiten Geschwindigkeitsbereich zur Simulation dynamischer Experimente eignen.

Schlüsselworte: Tribokorrosion, Eindruck, Erosion, Partikel Kantigkeit, kinetische Energie

Introduction

Solid particle erosion remains a problem for the engineering industry, due to the down time costs required to replace or repair worn components. Previous investigations in erosion processes have been carried out both in gaseous and wetted conditions, most notably by using the jet impingement and slurry pot apparatuses [1-3]. General findings revealed plastic deformation under normal impingement angles and ploughing/cutting under oblique impingement angles for ductile materials [4]. It was also shown that spherical particles are more efficient in producing plastic deformation wear whereas angular particles are more efficient in cutting and ploughing type of wear[5,6]. However, the experiments carried out under dynamic conditions produce erosion surfaces that are inevitably chaotic in nature, making it complicated to determine true contact conditions and wear mechanisms. These experiments are subjected to some disadvantages such as difficulties in controlling the hydrodynamic conditions, leading to inaccuracies in particle velocity and impact angle. Single particle impact experiments have been carried out by Hutchings in order to investigate wear mechanisms [4,6]. It was demonstrated that three types of particle surface interactions are responsible for erosive wear, namely plastic deformation, ploughing and cutting wear. Burstein and Sasaki also carried out single impact experiments under slurry conditions [7]. Under normal impact, plastic deformation wear has resulted in the breakdown of passive films on stainless steels, exposing the bare metal to corrosive attack. Adler and Doğan [8] investigated the strain hardening rate of austenitic white cast irons under single impact erosion at velocities up to 200 ms^{-1}. They have related the impact crater size to the energy absorbed by plastic and elastic deformation, through indentation experiments using WC-Co spheres. It was shown that the estimation of impact velocity under erosion can be gauged from indentation load-displacement relationship. The current work presents a novel micro-indenter, constructed for simulating random single particle impacts under erosion conditions. The objective is to investigate particle-surface contact conditions when an aluminium surface is indented by particles used in dynamic erosion experiments.

* Max-Planck-Institut für Eisenforschung, Max-Planck-Strasse 1, 40237 Düsseldorf, Germany

Experimental procedures

Micro-indentation rig construction

As seen in *Figure 1*, the micro-indentation rig consists of three sections. The first section includes an indenter tip, attached to a force sensor and XYZ manipulator. The XYZ manipulator was used for positioning the indenter and moving it close to the sample surface. Below the indenter tip, a sample holder was fixed on top of a z-direction piezo actuator, which is in turn attached to a stationary base plate. The second section consists of electronics that controls and records the responses from the force sensor and the piezo actuator. The force sensor being one loop of a wheatstone bridge was connected to a differential amplifier and its output to an analogue to digital converter (ADC). The amplifier generates a tuning voltage for the force sensitive thin film metal resistor, amplifies the detuning and generates force proportional voltage. Amplified analogue voltage signals were then digitised by a Labjack U12 (12-bit) ADC before being recorded by a computer via the USB interface. The response voltage was calibrated into load (mN) by carrying out initial indentations on a microbalance (Sartorius BL3100) with a resolution of $\pm$ 1 mN. The z-direction piezo actuator was connected to the EDA3 Digital interface board and ENV40C power supply/amplifier modules (Piezosystem Jena). The piezo power supply/amplifier can produce a voltage between 0 and 150 V, resulting in a maximum displacement of 80 μm and a resolution of 20 nm. Actuation and displacement information of the piezo actuator was controlled by the same computer via a GPIB interface. Control software, written in Agilent VEE, were utilised for displacing the piezo and for obtaining load data which was subsequently saved in an ASCII format.

In order to simulate the contact mechanics during particle impact, particles used commonly in dynamic erosion experiments [9-11] have to be fitted onto the indenter tip. In the following experiments, sintered zirconium oxide (ZrO_2) beads with a mean diameter of 125 μm and angular silicon carbide (SiC) particles (shown in *Figure 2*) were mounted onto stainless steel rods by high strength epoxy adhesives. Scanning electron micrographs showing the mounted ZrO_2 bead and the SiC particles on stainless steel tips are shown in *Figure 3*.

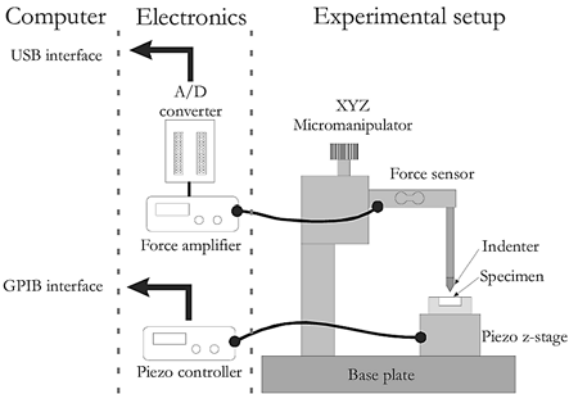

Figure 1. Micro indenter construction, shown in 3 sections, experimental setup, controlling electronics and computer (data acquisition).

Abbildung 1. Schematische Darstellung des Mikroindenters unterteilt nach den 3 Funktionseinheiten: experimenteller Aufbau, Steuer- und Regelelektronik, Computeranschluss mit Messdatenerfassung

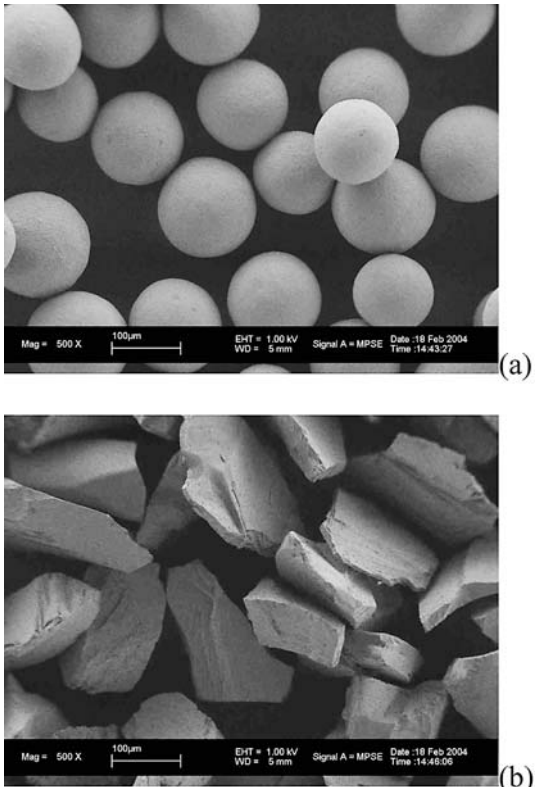

Figure 2. Micrograph of (a) spherical sintered zirconium oxide (mean diameter 125 μm) and (b) angular silicon carbide particles used for indentation experiments.

Abbildung 2. Mikroskopbilder der (a) kugelförmigen gesinterten Zirkoniumoxidpartikel (durchschnittlicher Durchmesser 125 μm) und der (b) scharfkantigen Siliciumkarbidpartikel die in dieser Arbeit zum Einsatz kommen.

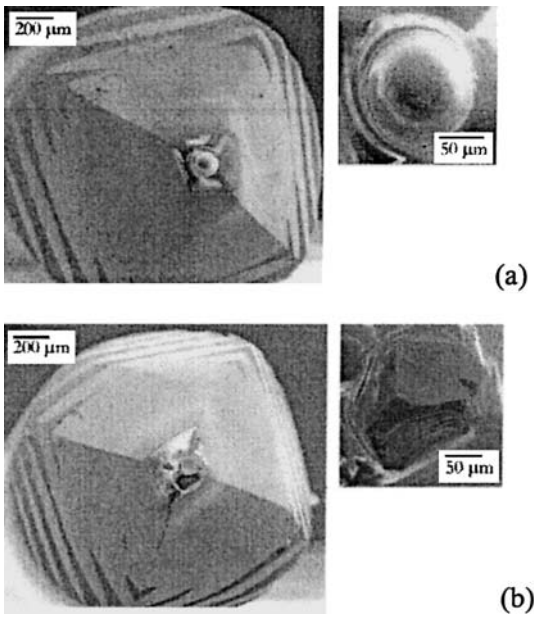

Figure 3. Micrographs showing single (a) zirconium oxide and (b) silicon carbide particles, mounted onto stainless steel tips used in indentation experiments.

Abbildung 3. Mikroskopaufnahmen einzelner (a) Zirkoniumoxid und (b) Siliciumkarbidpartikel, die für Indenterexperimente auf einer Stahlnadel montiert wurden.

 # 37549 / WILEY-VCH / M+W / Artikel T 832 cyan magenta yellow black **07. 01. 2005 t:/3b2/Muw/Umbruch/01-2005/t832.3d pS# 2**

Indentation experiments

High purity (99.99 %) aluminium samples were used in the indentation experiments. The samples were cut into small plates measuring 7 × 12 × 1 mm, subsequently ground by SiC embedded paper and polished with diamond suspensions until the final stage (suspended 0.5 μm fine Al_2O_3 particles) in order to obtain a reasonably flat surface with $R_a < 100$ nm. The polished sample was subsequently mounted on the sample holder and attached to the piezo actuator.

Indentation loads ranging between 50 and 1800 mN were used to investigate gross surface deformations under particle impact at normal impingement angles. Due to the limited vertical displacement of the piezo stage, indentations above 100 mN were simply carried out by displacing the micro-manipulator manually. The indenter was moved towards the sample slowly until the required loading was reached. For indentations below 100 mN, the indenter tip was initially brought to within 5 μm of the polished surface with the aid of a micro-manipulator and a camera. It was then left stationary while the sample surface was moved towards the indenter, with the help of the piezo actuator, at a constant displacement rate of 5656 nm s^{-1}. In all experiments, the indenter was allowed to remain in contact for 20 s when the target load was reached, so that full plastic deformation could occur. The sample preparation and indentation experiment explained above have been carried out in accordance with the EN 6507-1 (ISO 6507-1: 1997) standards [12].

Results and discussion

Scanning electron microscope images of the indentation craters are shown in *Figure 4*. The craters were produced by a series of indents between 50 and 1800 mN, at a 90° angle. It is evident that for both types of particles, the crater size increased with the loading. Indents were barely visible at a load of 50 mN, indicating that a threshold loading is required before plastic deformation can occur. The craters were apparently produced by plastic flow of aluminium towards the periphery of the contact point, resulting in a residual crater. Crater morphologies were shown to match the types of particles used; irregular impressions were formed by the angular SiC particles while circular impressions were formed by spherical particles. Pile-up of aluminium was also observed at the crater edge for both types of indents, especially at loads above 1000 mN. These pile-up formations have also been observed by other workers in single particle impact erosion experiments, on elastic-plastic materials such as aluminium [11], white cast iron [8] and brass [13]. It has been suggested that these highly strained plastic deformations are work hardened and are very likely to be removed by subsequent impacts under erosion conditions. The pile-ups can also result in plastic lip formation, often observed in the erosion morphology of ductile materials [14].

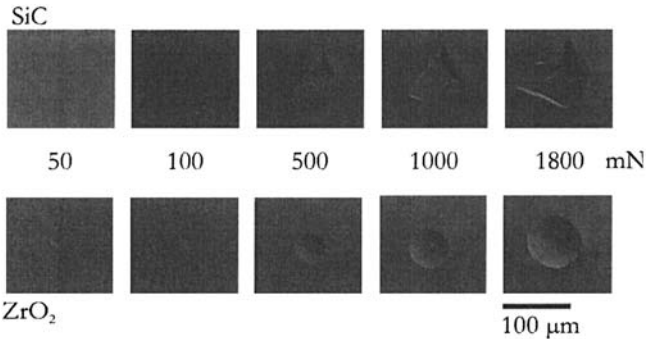

Figure 4. Series of indentation craters produced at indentation loads between 50 and 1800 mN, from angular SiC and spherical ZrO_2 indenter tips.

Abbildung 4. Serie von Eindruckkratern unter Kräften zwischen 50 und 1800 mN, jeweils von genau einem scharfkantigen SiC Partikel (obere Reihe) und einer ZrO_2-Kugel (untere Reihe).

Crater contact areas were estimated for both types of particles. For the ZrO_2 particles, approximation of the contact area was carried out using geometrical calculations:

$$A_{contact} = 2\ \pi\ r\ h \tag{1}$$

Where r = ZrO_2 sphere radius (62.5 μm) and h = crater depth, calculated from the residual crater radius by the following equation:

$$h = r - \sqrt{r^2 - r_1^2} \tag{2}$$

Where r_1 = crater radius, observed in the SEM.

Due to the irregular nature of craters produced by the SiC particles, area estimation was confined to residual horizontal surface areas. Comparison of area between craters produced by both types of indenter particles are shown in *Table* 1. It is possible to postulate that deformations at low loads are dominated by the spherical particles, while the angular particles deform more at higher loading conditions. Low contact areas for SiC particles at low loads are possibly caused by its asymmetrical geometry, giving rise to an uneven contact area, as opposed to the more uniform spherical ZrO_2 particles [10,13]. Microscopic examination indicates that maximum load bearing contact areas between the angular particles and the aluminium surface might be limited to the crater rim, where it was most plastically deformed. It is therefore possible that the effective contact area was limited to the sharper edges of the SiC particle, which can be approximately 30 to 40 % smaller than the crater area. The smaller effective contact area could produce contact pressures up to 50 % higher than those achieved by spherical particles, leading to higher deformation efficiencies. This phenomenon could possibly explain the larger horizontal crater areas produced by SiC particles at higher loads.

Ni et al. [15,16] carried out indentation experiments on nickel titanium shape memory alloys, using Berkovich and spherical diamond tips. The recovery ratio for spherical indentations was reported to be larger than those from sharp Berkovich tips for any given strain rate. They also demonstrated that plastic strain under a conical indenter is approximately 3 times higher than that under a spherical indenter, indicating that sufficiently large volume of material directly below a pyramidal indenter is so highly strained that significant deformation occurs through dislocation motion. The stress at sharp indenter tip rises to a theoretically infinite value at the apex unless plastic deformation occurs, whereas maximum stress under spherical indenter remains finite. Such explanations support the findings of higher deformation efficiency for sharp particles, subsequently resulting in higher erosion rates. Nonetheless, under real erosion conditions, variation in particle contact angle and rotation can further contribute to the erosion efficiency of sharp particles due to the added effects of cutting wear [6,17].

37549 / WILEY-VCH / M+W / Artikel T 832 cyan magenta yellow black 07. 01. 2005 t:/3b2/Muw/Umbruch/01-2005/t832.3d pS# 3

Table 1. Analysis of crater area with respect to various loads used in the indentation experiments.
Tabelle 1. Analyse der Kraterfläche als Funktion der in den Eindruckexperimenten verwendeten Kraft.

Load / mN	ZrO_2			SiC
	Crater depth / μm	Crater diameter / μm	Contact area /μm^2	Horizontal area /μm^2
50	0.4	13.6	145.7	68.4
100	0.7	18.8	279.2	191.4
500	3.8	43.0	1498.0	1624.9
1000	7.0	57.4	2740.7	3194.7
1800	12.9	76.0	5057.5	5475.0

The amount of work done by individual indentations with spherical ZrO_2 particles was also estimated using the following equation [8]:

$$W_{indentation} = F\ x \tag{3}$$

With F = indentation load (mN) and x = plastic deformation depth (See Table 1).

Work done during an indentation experiment can then be correlated with the kinetic energy during particle impact under dynamic conditions:

$$W_{indentation} = \text{Kinetic energy } (E_k) = \frac{1}{2}mv^2 \tag{4}$$

Where m = particle mass and v = impact velocity

Particle mass, m, can be calculated by multiplying the particle volume and density:

$$m = \rho\ V = \frac{4}{3}\rho\ \pi\ r^3 \tag{5}$$

Where $\rho = ZrO_2$ particle density (5700 kgm^{-3}) and $r = ZrO_2$ particle radius (62.5 μm, based on a mean diameter of 125 μm).

Hence,

$$W_{indentation} = \frac{2\pi}{3}\rho\ r^3\ v^2 \tag{6}$$

By using Equation 6, it is possible to estimate the velocity required to result in a plastically deformed crater under dynamic erosion conditions. The indentation loads used, work done and estimated velocities are shown collectively in *Figure 5*. A linear curve fit reveals that micro indentation can be successfully utilised for simulating the impact velocity of ZrO_2 particles under dynamic conditions, all within a reasonably short time and with a straightforward equipment set up. These results are similar to those obtained by indentation and erosion of white cast iron with WC-Co spheres [8], the load-velocity relationship was found to be valid for velocities up to 200 ms^{-1}. Equation 6 also allows the simulation of erosion impact velocities for particles of different sizes and densities; increment in particle size or density will lead to a similar increase in the work done, resulting in larger impact velocity slopes in Figure 5. However, this type of simulation is limited to particles of uniform shapes. It should also be noted that under prolonged erosion and repeated impacts, the target material surface may be subjected to strain hardening, leading to a change in erosion mechanisms such as brittle cracking. The relationship between indentation load and velocity might then not be as accurate, as part of the work done will be used for brittle crack formation.

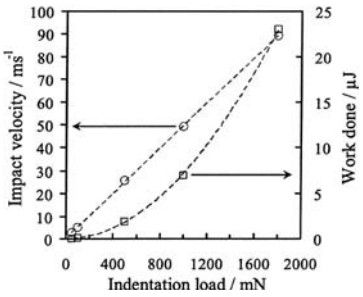

Figure 5. Estimation of ZrO_2 particle impact velocity from indentation load, based on equating the indentation work done with impact kinetic energy under dynamic erosion experiments.

Abbildung 5. Abschätzung des Zusammenhanges zwischen ZrO_2 Partikel Geschwindigkeit und Eindruckkraft. Die Berechnung erfolgt durch Gleichsetzen der Arbeit im statischen Eindruckexperiment mit der kinetischen Einschlagenergie im dynamischen Experiment.

Conclusions

1. A novel micro indenter has been constructed for tribological experiments, allowing indentations utilising spherical and angular erodent particles to be carried out. Indentations were performed on an aluminium surface, with loads varying between 50 and 1800 mN.
2. Two types of experiments have been carried out, based on two different types of particle geometries used in dynamic erosion experiments. Under normal angle impact conditions, angular SiC particles produced higher plastic deformation volume than the spherical ZrO_2 particles. This is possibly due to higher contact pressures from the angular particles, as the effective contact area might be smaller than those of spherical particles.
3. Analysis of the wear crater area revealed that the initial deformation volumes of angular particles are smaller than those of spherical particles. This phenomenon is reversed at higher loading, indicating the effect that the complexities of particle geometry and effective contact area have on the erosion mechanism.

4. The work done during indentation can be utilised to estimate particle impact velocities under dynamic erosion. The linear relationship between indentation load and impact velocity allows contact conditions during particle impact to be investigated with relative ease. The estimation of impact velocity is only valid for non-work hardened surfaces that are not subjected to brittle cracking.

Acknowledgement

KST gratefully acknowledges the financial support from the Max Planck Society through a Max Planck Fellowship.

References

1. R.J.K. Wood, D.W. Wheeler, *Wear* **1998**, *220*, 95.
2. J.B. Zu, I.M. Hutchings, G.T. Burstein, *Wear* **1990**, *140*, 331.
3. H.M. Clark, *Wear* **1995**, *186–187*, 465.
4. I.M. Hutchings, Tribology - Friction and wear of engineering materials, Edward-Arnold, London **1992**.
5. I.M. Hutchings, R.E. Winter, *Wear* **1974**, *27*, 121.
6. I.M. Hutchings, 'Mechanisms of the erosion of metals by solid particles' Erosion: Prevention and Useful Applications, ASTM STP 664, 59–76, ASTM, **1979**.
7. G.T. Burstein, K. Sasaki, *Electrochim. Acta* **2001**, *46*, 3675.
8. T.A. Adler, O.N. Doğan, *Wear* **1997**, *203–204*, 257.
9. A.J. Sparks, I.M. Hutchings, *Wear* **1993**, *162–164*, 139.
10. S.L. Palasamudram, S. Bahadur, *Wear* **1997**, *203–204*, 455.
11. Y.I. Oka, K. Nagahashi, *Wear* **2003**, *254*, 1267.
12. 'DIN-Taschenbuch 19: Materialprüfnormen für metallische Werkstoffe', Deutsches Institut für Normung e.V., Berlin, **2000**.
13. M. Dundar, O. Keles, O.T. Inal, *J. Mater. Sci.* **2000**, *35*, 3989.
14. A.V. Levy, *Wear* **1986**, *108*, 1.
15. W.Y. Ni, Y.T. Cheng, D.S. Grummon, *Surf. Coat. Technol.* **2004**, *177–178*, 512.
16. W.Y. Ni, Y.T. Cheng, D.S. Grummon, *Appl. Phys. Lett.* **2002**, *80*, 3310.
17. M. Papini, J.K. Spelt, *Int. J. Mech. Sci.* **2000**, *42*, 991.

Corresponding author: Dr. A. W. Hassel, *Max-Planck-Institut für Eisenforschung, Max-Planck-Strasse 1, 40237 Düsseldorf, Germany,* Fax: +49-211-6792-218, e-mail: hassel@elchem.de

Received in final form: 10/12/04 [T 832]